

Influence of steel corrosion on axial and eccentric compression behavior of coral aggregate concrete column

Bo DA^{a,b,c,d}, Yan CHEN^b, Hongfa YU^{e*}, Haiyan MA^{e*}, Bo YU^d, Da CHEN^{b,c}, Xiao CHEN^a, Zhangyu WU^c, Jianbo GUO^e

^a State Key Laboratory of Silicate Materials for Architectures, Wuhan University of Technology, Wuhan 430070, China

^b College of Harbour, Coastal and Offshore Engineering, Hohai University, Nanjing 210098, China

^c Key Laboratory of Coastal Disaster and Defence of Ministry of Education, Hohai University, Nanjing 210098, China

^d Guangxi Key Laboratory of Disaster Prevention and Engineering Safety, Guangxi University, Nanning 530004, China

^e Department of Civil and Airport Engineering, Nanjing University of Aeronautics and Astronautics, Nanjing 210016, China

*Corresponding author. E-mails: yuhongfa@nuaa.edu.cn; mahaiyan@nuaa.edu.cn

© Higher Education Press 2021

ABSTRACT To study the behavior of coral aggregate concrete (CAC) column under axial and eccentric compression, the compression behavior of CAC column with different types of steel and initial eccentricity (e_i) were tested, and the deformation behavior and ultimate bearing capacity (N_u) were studied. The results showed that as the e_i increases, the N_u of CAC column decreases nonlinearly. Besides, the steel corrosion in CAC column is severe, which reduces the steel section and steel strength, and decreases the N_u of CAC column. The durability of CAC structures can be improved by using new organic coated steel. Considering the influence of steel corrosion and interfacial bond deterioration, the calculation models of N_u under axial and eccentric compression were presented.

KEYWORDS coral aggregate concrete column, axial compression, eccentric compression, steel corrosion, calculation model

1 Introduction

The application of CAC column has important value of engineering in the tropical island-reef engineering [1–3]. However, coral and seawater contain large amounts of Cl^- quickly leading to the corrosion of steel bar, which severely affects the durability of CAC structure [4,5]. So, it is necessary to conduct experimental investigation on compressive behavior of CAC column.

Wattanachai [6] found that the apparent Cl^- diffusion coefficient of CAC was greater than that of ordinary aggregate concrete (OAC) at the same mix proportion. Zhang [7] studied the mechanical property of CAC beam and column, and the calculation model of bearing capacity was established. Still, the ordinary steel has been severely corroded, and the influence of steel corrosion

had not been analyzed. Yu et al. [8] and Da et al. [9] researched the durability status of building structures in the Xisha Islands, and the cracking, spalling, steel corrosion and Cl^- diffusion of CAC structures were analyzed. Da et al. [10] studied the steel corrosion behavior in CAC, and the anti-corrosion method of CAC was obtained. Yang et al. [11] studied the bond behavior between steel and CAC, and found that bond strength decreases linearly with the increase of steel diameter. Ma et al. [12] studied the mechanical property of CAC beam and column, and applicability of the calculation model of OAC and lightweight aggregate concrete (LAC) in CAC were discussed. Therefore, this paper reports the effect of steel corrosion on compressive behavior of CAC column.

To study the behavior of CAC column under axial and eccentric compression, 12 columns (2 OAC columns and 10 CAC columns) with different steel type and initial eccentricity were designed. The compression behavior of

CAC column were analyzed. Considering the influence of steel corrosion and interfacial bond deterioration, the calculation models of N_u under axial and eccentric compression were presented.

2 Experiment

2.1 Preparation method

The size of CAC column is 200 mm × 240 mm × 1500 mm (Fig. 1). The mix proportion of CAC is coral : coral sand : cement : fly ash : slag : seawater : inhibitor : water reducer = 300 : 700 : 780 : 70 : 150 : 264 : 30 : 6 kg/m³. Among them: the concrete strength is C60, the steel is ordinary steel (A), new organic coated steel (B), 316 stainless steel (C), the initial eccentricity (e_i) are 0, 70, 160 mm, the seawater is 3.5% NaCl solution. According to the GB/T 50081-2002—Standard for Test Method of Mechanical Properties on Ordinary Concrete [13], the cube compressive strength (f_{cu}) and axial compressive strength (f_c) of CAC were tested using three concrete specimens with the side length of 100 mm × 100 mm × 100 mm and 100 mm × 100 mm × 300 mm, where the f_{cu} and f_c value was calculated by the average strength value of the three concrete specimens. According to the JGJ 12-2006—Specification for Design of Lightweight Aggregate Concrete Structures [14], the flexural

compressive strength (f_{cm}) was calculated, $f_{cm} = 1.05f_c$.

Tables 1 and 2 are the basic parameters of coral aggregates and CAC column. Among them: f_y is tensile strength of steel (MPa), ω is mass loss rate of steel (%), ω_{sm} is maximum section loss rate of steel (%). Besides, the longitudinal steel is 4Φ20 ribbed steels, and the stirrups is Φ8 plain steel.

2.2 Test method

2.2.1 Rebar corrosion

According to the GB/T 50082-2009—Standard for Test Methods of Long-term Performance and Durability of Ordinary Concrete [15], the mass loss rate of steel (ω) in concrete was tested in this work. The rust removal method: pickling sample with 12% HCl solution, rinsing it with clear water, neutralizing it with saturated Ca(OH)₂

Table 1 Basic parameters of coral sand and coral

basic parameters	coral	coral sand
bulk density (kg·m ⁻³)	1000	1115
apparent density (kg·m ⁻³)	2300	2500
chloride content (%)	0.074	0.112
mud content (%)	–	0.5
fineness modulus	–	2.9

Table 2 Basic parameters of CAC column

No.	concrete type	steel type	e_i (mm)	f_{cu} (MPa)	f_c (MPa)	f_{cm} (MPa)	f_y (MPa)	ω (%)	ω_{sm} (%)	N_{cr} (kN)	N_u (kN)
L3-1	OAC	B	160	62.8	51.8	54.4	530	–	–	110	410
L3-2		B	160	61.8	51.0	53.6	530	–	–	100	470
L4-2	CAC	C	160	104.1	81.8	85.9	922	0.10	0.13	130	570
L5-1		A	160	104.9	82.4	86.5	530	2.12	2.76	90	700
L5-2		A	160	104.6	82.1	86.2	530	2.12	2.76	110	720
L6-1		B	160	104.6	82.1	86.2	530	0.53	0.69	120	650
L6-2		B	160	103.2	81.1	85.2	530	0.53	0.69	100	570
A7-1		B	0	104.8	82.3	86.4	530	0.53	0.69	–	810
A7-2		B	0	103.9	81.6	85.7	530	0.53	0.69	–	1900
S8-1		B	70	104.7	82.2	86.3	530	0.53	0.69	360	1540
S8-2		B	70	104.3	81.9	86.0	530	0.53	0.69	300	1550

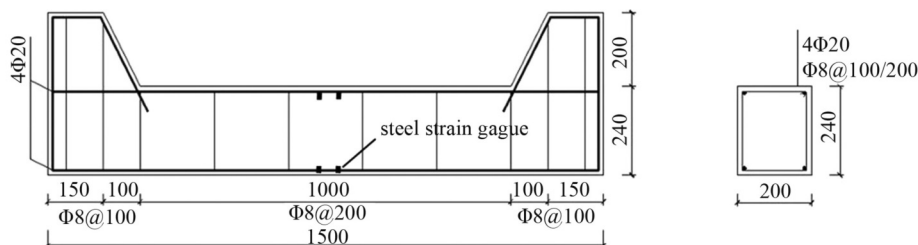


Fig. 1 Dimension and steel detail of CAC column (mm).

solution, and finally rinsing it with clean water. Wipe and then dry it, which is stored for at least 4 h, and then weigh it with an analytical balance. The equation to calculate the ω is as follows:

$$\omega = \frac{d \cdot \rho_w - m}{d \cdot \rho_w} \times 100\%, \quad (1)$$

where ω is the mass loss rate of steel (%); d is the diameter of steel (mm); ρ_w is the linear density of steel ($\text{g} \cdot \text{mm}^{-1}$); m is the mass of steel after rust removal (g).

2.2.2 Axial compression

Figure 2 is schematic diagram of compression behavior test of CAC column. To measure axial deformation of the column, 1 displacement sensor is arranged on the loading plate at the bottom of tester. To measure lateral deformation of the column, 2 displacement sensors are arranged on the center of two sides of column. To measure strain of the steel (Fig. 1), 2 steel strain gauges are attached to the midspan of longitudinal steel. To measure strain of the concrete, 1 transverse and 1 longitudinal concrete strain gauge are attached to the center of two sides of column. Besides, DH3818-2 strain indicator, 200 t load sensor and SW-LW-201 crack detector are used to collect strain, stress and crack width. The loading method is according to the GB/T 50152-2012—Standard for Test Method of Concrete Structures [16].

2.2.3 Eccentric compression

To measure lateral deformation of the column, 5 displacement sensors are arranged on the tension side of column. To measure strain of the concrete, 1 transverse and 1 longitudinal concrete strain gauge are attached to the middle of compression, tensile side of column. The arrange method of other steel/concrete strain gauges and data acquisition methods are consistent with that of the axial compression.

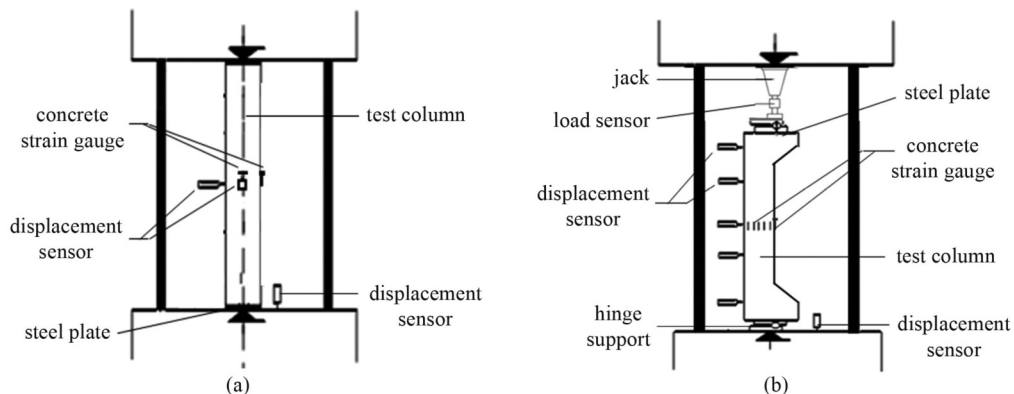


Fig. 2 Schematic diagram of compression behavior test of CAC column: (a) axial compression; (b) eccentric compression.

3 Results and analysis

3.1 Failure mode

3.1.1 Axial compression

Figure 3 is failure mode of CAC column. It is shown that concrete and steel strain are the same when the load is small. As the increase of load, the strain growth rate of concrete/steel are accelerated, and small vertical cracks begin to appear in the surface of column. As the load continued to increase, the crack width enlarged continuously, and gradually extended to the middle of the column. When failure is approaching, the vertical cracks increased. Finally, a large splitting crack appears in the longitudinal direction of the column, the concrete is crushed, the longitudinal steel is yielded, and the CAC column fails.

3.1.2 Eccentric compression

As shown in Fig. 3, when the load is small, the law of eccentric compression is consistent with the axial compression. As the increase of load, the cracks appear in the tensile zone of column, and the crack width increased gradually. As the load continued to increase, when the $e_i = 70$ mm, due to the concrete crushing in the middle section on the compression side, the CAC column fails, it is a small eccentric compression failure. When the $e_i = 160$ mm, due to the tensile steel is yielded, and concrete crushing on the compression side, the CAC column fails, it is large eccentric compression failure. Compared to the small eccentric compression failure, the range in the compression zone is smaller, but the crack length, width and spacing are larger.

3.2 Deformation

3.2.1 Load–displacement

Figure 4 is load–displacement curves of CAC column. It

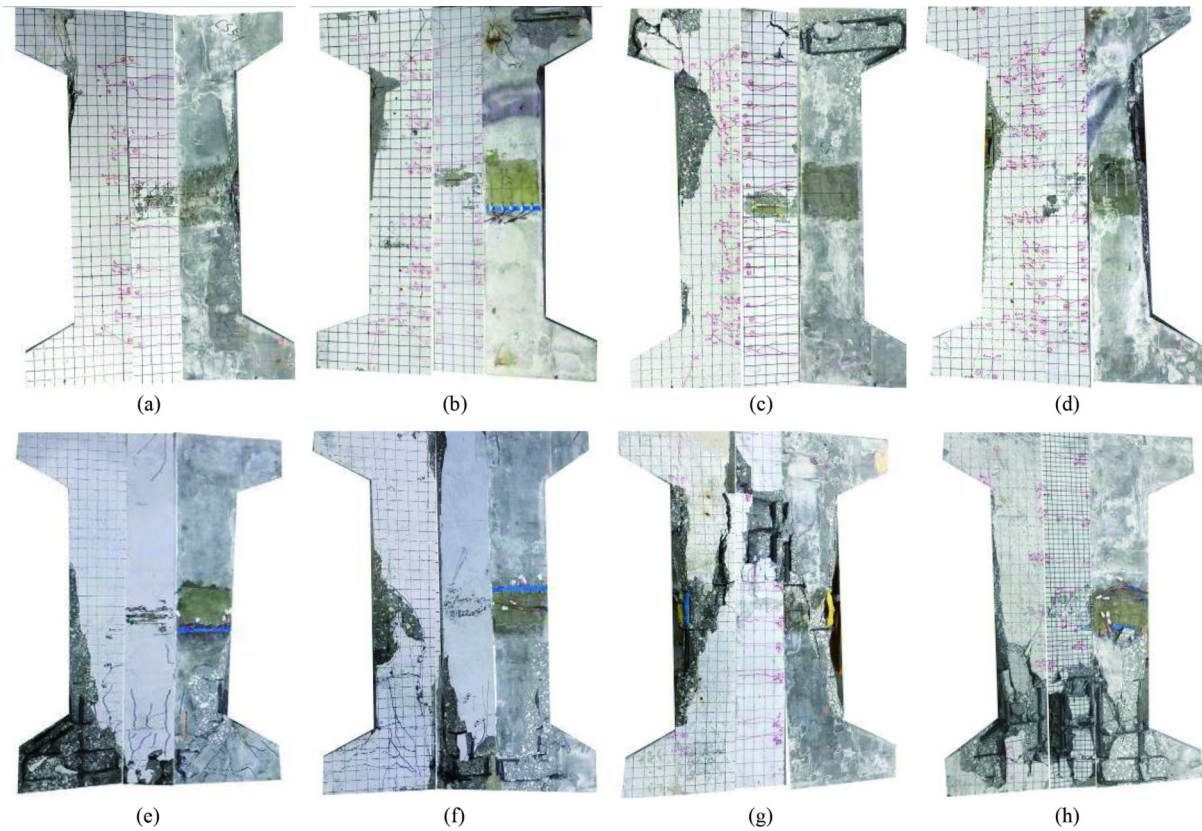


Fig. 3 Failure mode of CAC column: (a) L3-1; (b) L3-2; (c) L6-1; (d) L6-2; (e) A7-1; (f) A7-2; (g) S8-1; (h) S8-2.

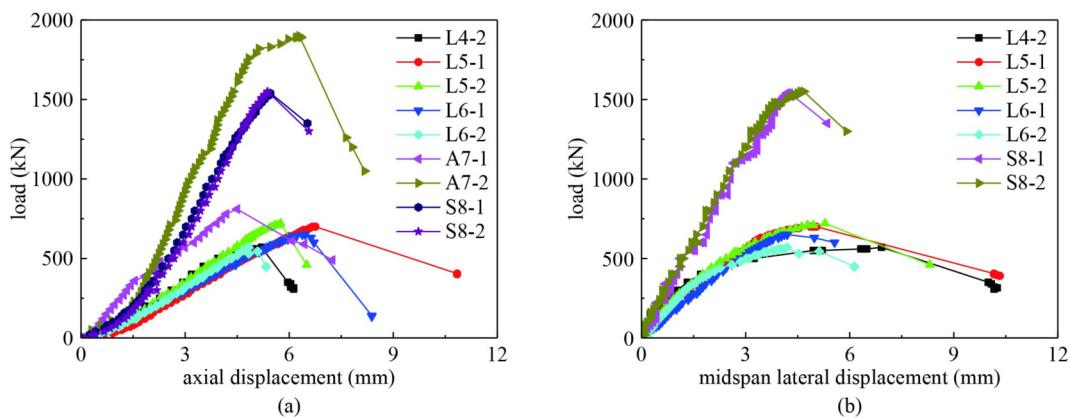


Fig. 4 Load–displacement curves of CAC column: (a) axial displacement; (b) midspan lateral displacement.

is shown that the axial and midspan lateral deformation of CAC column with different types of steel are as follows: $L4 < L5 < L6$, namely with the increase of steel strength, the axial and midspan lateral deformation decreased gradually. The reasons are that: 1) The N_u of CAC column is composed of concrete bearing capacity and steel bearing capacity. When the concrete strength is equal, with the increase of steel strength, the N_u increased gradually, indicating that the anti-deformation capacity increased gradually. 2) There is a protective coating on the surface of coated steel. In the loading process, more massive bond slip takes place between the steel and

concrete, the bonding strength decreased, and the axial deformation of L6-1 increased. 3) The axial deformation of L6-1 is less than that of L5-1. This is because there is lots of Cl^- in the CAC column, resulting in severely corrosion of ordinary steel, which reduces the steel strength and steel section [17], and decreases the N_u of CAC column.

Furthermore, as shown in Fig. 3, the axial and midspan lateral deformation of CAC column with different e_i are as follows: $A7 < S8 < L6$. Indicate that with the increase of e_i , the axial and midspan lateral deformation of CAC column increased gradually. This rule is same as that of

the OAC column [18].

3.2.2 Load-compressive strain

Figure 5 is load-compressive strain curves of CAC column. It is shown that: 1) The concrete and steel strain of CAC column with different types of steel is as follows: $L4 < L5 < L6$. The reason is that the f_y of 316 stainless steel (L4) is higher than that of ordinary steel (L6). Thus, the anti-deformation capacity of L4 was the strongest, the concrete and steel strain of L4 was the smallest. 2) The concrete and steel strain of CAC column with different e_i is as follows: $A7 < S8 < L6$, namely with the increase of e_i , the concrete and steel strain of CAC column increased gradually. This rule is same as that of the OAC column [18].

3.2.3 Load-tensile strain

Figure 6 is load-tensile strain curves of CAC column. It is shown that: 1) The ultimate tensile strain (ϵ_{su}) of longitudinal steel of L5-1, L6-1 are 3679 and 3298 $\mu\epsilon$, respectively. However, the yield strain (ϵ_s) of ordinary steel is 2524 $\mu\epsilon$. Indicates that when bearing capacity of CAC column reached N_u , the longitudinal tensile steel of L5-1 and L6-1 has yielded. 2) Compare the load-tensile

strain of L5-1 and L6-1, found that when the flexural cracks of CAC column occurred, the longitudinal tensile strain of L5-1 and L6-1 increased rapidly at 85 and 90 kN (Table 2).

3.3 Bearing capacity

3.3.1 Influence of initial eccentricity

Figure 7 is N_u of CAC column. It is shown that the N_u of L6-1, L6-2, A7-1, A7-2, S8-1, S8-2 are 650, 570, 810, 1900, 1540, and 1550 kN, respectively (Note: in the test process, due to the end of A7-1, it is crushed prematurely, the N_u was significantly low, and A7-1 was not considered in this study). Therefore, for the CAC column with same concrete strength, when the e_i increased from 0 to 70 mm, N_u decreased by 18.7%. When the e_i increased from 70 to 170 mm, N_u decreased by 60.5%. Indicates that with the increase of e_i , the N_u decreased nonlinearly.

3.3.2 Calculation and analysis

3.3.2.1 Comparison of different models

1) Axial compression:

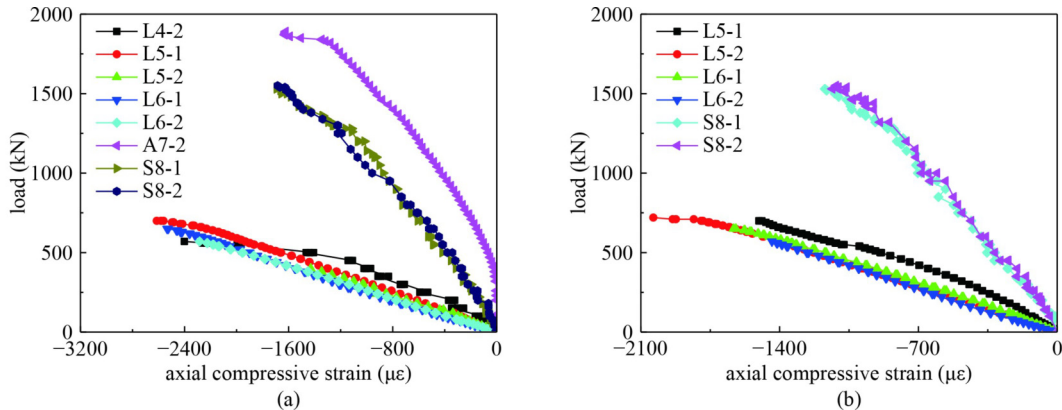


Fig. 5 Load-compressive strain curves of CAC column: (a) concrete; (b) steel.

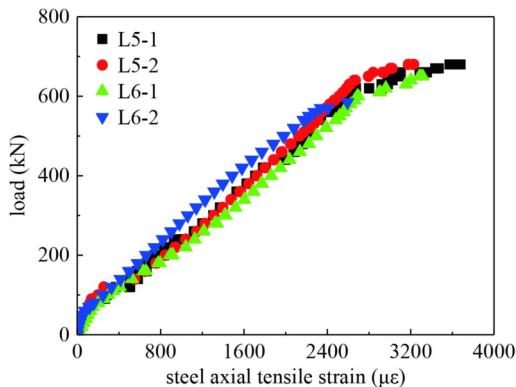


Fig. 6 Load-tensile strain curves of CAC column.

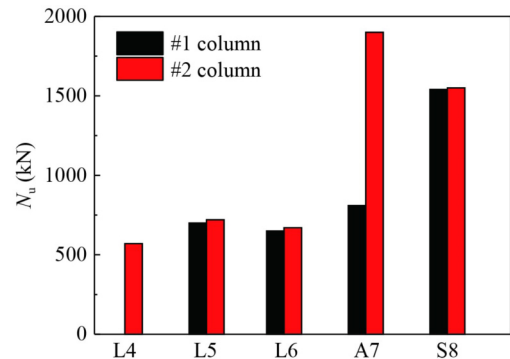


Fig. 7 Ultimate bearing capacity of CAC column.

$$\text{GB 50010-2010 : } N_u = 0.9\varphi(f_c A + f'_y A'_s), \quad (2)$$

$$\text{JGJ 12-2006 : } N_u = \varphi(f_c A + f'_y A'_s), \quad (3)$$

$$\text{EN-1992 : } N_u = \beta_2 \beta_3 f_c A + f'_y A'_s, \quad (4)$$

$$\text{ACI 318-1999 : } N_u = 0.8\varphi(\gamma f_c (A - A'_s) + f'_y A'_s), \quad (5)$$

where φ is stability coefficient. For the GB 50010-2010, $\varphi = 1$; for the JGJ 12-2006, $\varphi = 0.97$; for the ACI 318-1999, $\varphi = 0.7$; f_c is concrete axial compressive strength (MPa); f_y, f'_y are steel tensile, compressive strength (MPa); A is component sectional area (mm^2); A_s, A'_s are longitudinal steel sectional area in tensile, compression zone (mm^2); β_2, β_3 are stress, height coefficient; γ is strength difference coefficient.

Using Eqs. (2)–(5), the N_u of CAC column as shown in Fig. 8 and Table 3. The mean of N_u^c/N_u^t are 1.401, 1.450, 1.194, and 0.794, the standard deviations are 0.485, 0.551, 0.229, and 0.251, the variation coefficients are 0.346, 0.380, 0.192, and 0.335, respectively. It is shown that a large error between N_u^c and N_u^t . The N_u^c of CAC column calculated according to the ACI 318-1999 [19] is lower than N_u^t , indicates that this method is conservative. However, the N_u^c calculated according to the JGJ 12-2006 [20], GB 50010-2010 [21] and EN-1992 [22] are higher than N_u^t , indicates that these methods are not safe.

2) Small eccentric compression:

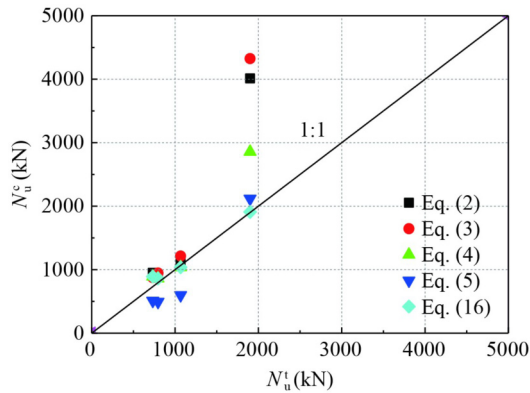


Fig. 8 N_u^c and N_u^t of CAC column under axial compression.

GB 50010-2010:

$$\begin{cases} N_u \leq \alpha_1 f_c b x + f'_y A'_s - \sigma_s A_s, \\ N_u e \leq \alpha_1 f_c b x (h_0 - x/2) + f'_y A'_s (h_0 - a'_s), \\ \sigma_s = \frac{x/h_0 - \beta}{\xi_b - \beta} f_y, \\ e = e_i + h/2 - a_s, \\ e_i = e_0 + e_a, \end{cases} \quad (6)$$

JGJ 12-2006:

$$\begin{cases} N_u \leq f_{cm} b x + f'_y A'_s - \sigma_s A_s, \\ N_u e \leq f_{cm} b x (h_0 - x/2) + f'_y A'_s (h_0 - a'_s), \\ f_{cm} = 1.05 f_{cu}, \\ e = \eta e_i + h/2 - a_s, \\ \eta = 1 + \frac{1}{1400(e_0/h_0)} \left(\frac{l_0}{h}\right)^2 \zeta_1 \zeta_2, \\ \zeta_1 = 0.5 f_c A/N, \\ \zeta_2 = 1.3 - 0.015 l_0/h, \\ e_i = e_0 + e_a, \\ e_a = 0.12(0.3h_0 - e_0), \\ \sigma_s = \frac{x/h_0 - 0.75}{\xi_b - 0.75} f_y, \end{cases} \quad (7)$$

EN-1992:

$$\begin{cases} N_u \leq \beta_3 f_c b (\beta_2 x) + f'_y A'_s - \sigma_s A_s, \\ N_u e \leq \beta_3 f_c b (\beta_2 x) (h/2 - \beta_2 x/2) + f'_y A'_s (h/2 - d_2) + \sigma_s A_s (d_1 - h/2), \\ e = e_i + h/2 - d_2, \\ \beta_2 = \begin{cases} 0.8, & f_{ck} < 50 \text{ MPa}, \\ 0.8 - (f_{ck} - 50)/200, & f_{ck} \geq 50 \text{ MPa}, \end{cases} \\ \beta_3 = \begin{cases} 1.0, & f_{ck} < 50 \text{ MPa}, \\ 1.0 - (f_{ck} - 50)/400, & f_{ck} \geq 50 \text{ MPa}, \end{cases} \\ \sigma_s = \frac{d - x}{x} \varepsilon'_u E_s, \end{cases} \quad (8)$$

ACI 318-1999:

Table 3 N_u^c and N_u^t of CAC column under axial compression (kN)

No.	N_u^t	Eq. (2)		Eq. (3)		Eq. (4)		Eq. (5)		Eq. (16)	
		N_u^c	N_u^c / N_u^t	N_u^c	N_u^c / N_u^t						
A7-1	810	4041	4.988	4355	5.376	2859	3.530	2133	2.634	1911	2.359
A7-2	1900	4012	2.112	4324	2.276	2856	1.503	2119	1.115	1909	1.005
CS-1 [7]	1067	1115	1.045	1215	1.138	1038	0.973	599	0.561	1038	0.973
CL1-1 [7]	796	916	1.151	946	1.189	861	1.082	493	0.620	861	1.082
CL2-1 [7]	733	950	1.297	876	1.196	892	1.217	512	0.698	892	1.217

$$\begin{cases} N_u \leq \gamma f_c b x + f_y' A_s' - \sigma_s A_s, \\ N_u e \leq \gamma f_c b x (h/2 - x/2) + f_y' A_s' (h/2 - a_s') + \sigma_s A_s (h_0 - h/2), \\ e = e_i + h/2 - a_s, \\ \sigma_s = \varepsilon_u' E_s \left(\frac{h_0}{x} - 1 \right), \end{cases} \quad (9)$$

where α_1 is stress diagram coefficient, $\alpha_1 = 0.975$ [23]; x , ξ_b are height, relative height in concrete compression zone (mm); σ_s is longitudinal steel stress (MPa); e is distance between axial stress point and tensile steel stress point (mm); e_i , e_0 , e_a are initial, gravity center, appendant eccentricity (mm); h_0 is section effective height (mm); a_s , a_s' are distance between section edge and tensile, compressive steel stress point (mm); β is fitting coefficient; f_{cm} is concrete flexural compressive strength (MPa), $f_{cm} = 1.05f_c$; η is eccentricity enhancement coefficient; l_0 is component length (mm); ζ_1 , ζ_2 are fitting coefficients, when $l_0/h < 20$, $\zeta_2 = 1$; d is sectional height (mm); d_1 , d_2 are concrete cover thickness in compression, tension zone (mm); ε_u' is concrete ultimate compressive strain ($\mu\varepsilon$), $\varepsilon_u' = 3400 \mu\varepsilon$ [23]; E_s is steel elastic modulus (GPa); see Eqs. (2)–(5) for other parameters.

Using Eqs. (6)–(9), the N_u of CAC column are shown in Fig. 9 and Table 4. The mean of N_u^c/N_u^t are 0.728, 1.009, 0.271, and 0.375, the standard deviations are

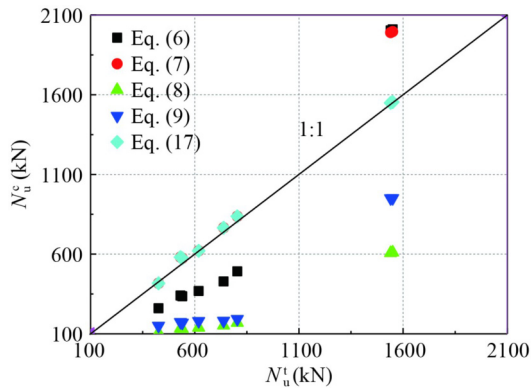


Fig. 9 N_u^c and N_u^t of CAC column under small eccentric compression.

0.319, 0.123, 0.073, and 0.153, the variation coefficients are 0.408, 0.112, 0.268, and 0.408, respectively. It is shown that a large error between N_u^c and N_u^t . The N_u^c of CAC column calculated according to ACI 318-1999, EN-1992 and GB 50010-2010 are lower than N_u^t , indicating that these methods are conservative. However, the N_u^c calculated according to JGJ 12-2006 is higher than N_u^t , indicating that this method is not safe.

3) Large eccentric compression:

GB 50010-2010:

$$\begin{cases} N_u \leq \alpha_1 f_c b x + f_y' A_s' - \sigma_s A_s, \\ N_u e \leq \alpha_1 f_c b x (h_0 - x/2) + f_y' A_s' (h_0 - a_s'), \\ e = e_i + h/2 - a_s, \\ e_i = e_0 + e_a, \\ e_a = 0.12(0.3h_0 - e_0), \end{cases} \quad (10)$$

JGJ 12-2006:

$$\begin{cases} N_u \leq f_{cm} b x + f_y' A_s' - f_y A_s, \\ N_u e \leq f_{cm} b x (h_0 - x/2) + f_y' A_s' (h_0 - a_s'), \\ e = \eta e_i + h/2 - a_s, \\ \eta = 1 + \frac{1}{1400(e_0/h_0)} \left(\frac{l_0}{h} \right)^2 \zeta_1 \zeta_2, \\ \zeta_1 = 0.5 f_c A / N, \\ \zeta_2 = 1.3 - 0.015 l_0 / h, \\ e_i = e_0 + e_a, \\ e_a = 0.12(0.3h_0 - e_0), \end{cases} \quad (11)$$

EN-1992:

$$\begin{cases} N_u \leq \beta f_c b (\xi_b d), \\ N_u e \leq \beta f_c b (\xi_b d) (h/2 - \xi_b d/2) + f_y A_s (d - d_2), \\ e = e_i + h/2 - d_2, \\ e_i = e_0 + e_a, \\ e_a = 0.12(0.3h_0 - e_0), \\ \beta = \begin{cases} 1.0, & f_{ck} < 50 \text{ MPa}, \\ 1.0 - (f_{ck} - 50)/400, & f_{ck} \geq 50 \text{ MPa}, \end{cases} \end{cases} \quad (12)$$

Table 4 N_u^c and N_u^t of CAC column under small eccentric compression (kN)

No.	N_u^t	Eq. (6)		Eq. (7)		Eq. (8)		Eq. (9)		Eq. (17)	
		N_u^c	N_u^c / N_u^t	N_u^c	N_u^c / N_u^t						
S8-1	1540	2003	1.301	1990	1.292	607	0.394	951	0.617	1549	1.006
S8-2	1550	2010	1.297	1997	1.288	610	0.394	951	0.614	1554	1.003
CS-2 [7]	804	492	0.612	837	1.041	169	0.210	193	0.240	837	1.041
CS-3 [7]	739	428	0.580	765	1.036	153	0.207	182	0.246	765	1.036
CS-4 [7]	619	368	0.596	621	1.004	139	0.224	180	0.292	621	1.004
CL1-2 [7]	531	340	0.640	581	1.093	133	0.250	174	0.327	581	1.093
CL1-3 [7]	426	260	0.611	417	0.978	105	0.247	150	0.352	417	0.978
CL2-2 [7]	540	336	0.621	574	1.062	130	0.241	170	0.314	574	1.062

ACI 318-1999:

$$\begin{cases} N_u \leq \gamma f_c b x + f_y' A_s' - f_y A_s, \\ N_u e \leq \gamma f_c b x (h/2 - x/2) + f_y' A_s' (h/2 - a_s') + f_y A_s (h_0 - h/2), \\ e = e_i + h/2 - a_s, \\ e_i = e_0 + e_a, \\ e_a = 0.12(0.3h_0 - e_0), \end{cases} \quad (13)$$

see Eqs. (2)–(5) for the parameters.

Using Eqs. (10)–(13), the N_u of CAC column are shown in Fig. 10 and Table 5. The mean of N_u^c/N_u^t are 1.087, 1.099, 0.667, and 0.650, the standard deviations are 0.040, 0.039, 0.041, and 0.039, the variation coefficients are 0.037, 0.035, 0.061, and 0.061, respectively. It is shown that a large error between N_u^c and N_u^t . The N_u^c of CAC column calculated according to EN-1992, ACI 318-1999 are lower than N_u^t , indicating that these methods are conservative. However, the N_u^c calculated according to JGJ 12-2006, GB 50010-2010 are higher than N_u^t , and this indicates that these methods are not safe.

3.3.2.2 Model optimization

Figure 11 is steel corrosion status in CAC column, it is

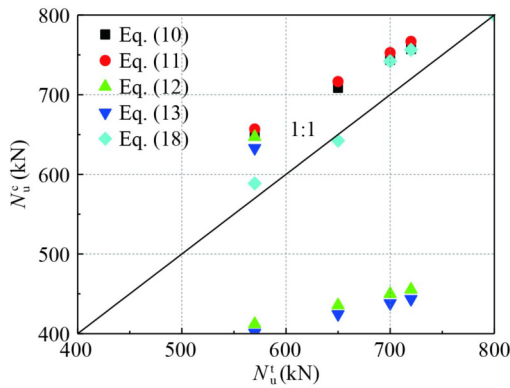


Fig. 10 N_u^c and N_u^t of CAC column under large eccentric compression.

shown that the ordinary steel (A) was severely corroded, the new organic coated steel (B) was partially corroded, but the 316 stainless steel (C) was not corroded. Figure 12 is the electrochemical test result of CAC structural, in which the concrete strength is C50, E_{corr} is self-corrosion potential (V), R_p is polarization resistance ($k\Omega \cdot cm^2$). It is shown that the anti-corrosion property of steel is $C > B > A$, which is consistent with the actual corrosion status of steel (Fig. 11). The reason is natural porous structure “defect” of coral and the large amount of Cl^- in seawater and coral itself easily lead to the corrosion of steel bars in CAC [10,24]. The corrosion of steel bars not only reduces the effective section and the mechanical properties of steel bars [25], but also degrades the bond property between steel bars and CAC [3], which seriously reduces the N_u of CAC column. Besides, Yuan et al. [17] proposed calculation formula of the comprehensive reduction coefficient (α):

$$\alpha = \alpha_2 \cdot \alpha_3 = \begin{cases} (1 - \omega_s)(1 - 1.608\omega_s), & 0 < \omega_s \leq 5\%, \\ (1 - \omega_s)(0.962 - 0.848\omega_s), & \omega_s > 5\%, \end{cases} \quad (14)$$

where α_2 , α_3 are steel section, strength reduction coefficient. See Table 2 for other parameters.

However, the steel is prone to pit in the marine environment. So, there is a minimum section of the steel, under the stress state, the position of minimum section (maximum section loss rate, ω_{sm}) is most likely to crack. Wang and Zhong [26] found that the mean section loss rate (ω_s) and ω_{sm} have an excellent linear relationship. Furthermore, Zhang et al. [25] found that the ω_s and ω_{sm} are nearly equal. So, use ω_{sm} to calculate the α :

$$\begin{cases} \omega_{sm} = 1.301\omega_s, \\ \alpha = \begin{cases} (1 - 1.301\omega)(1 - 1.608\omega), & 0 < \omega \leq 5\%, \\ (1 - 1.301\omega)(0.962 - 0.848\omega), & \omega > 5\%. \end{cases} \end{cases} \quad (15)$$

In addition, steel corrosion greatly weaken the bonding effect between steel bars and concrete, and cause the degradation of the bonding performance of reinforced concrete [25,27]. Therefore, the corrosion of steel bars

Table 5 N_u^c and N_u^t of CAC column under large eccentric compression (kN)

No.	N_u^t	Eq. (10)		Eq. (11)		Eq. (12)		Eq. (13)		Eq. (18)	
		N_u^c	N_u^c / N_u^t								
L4-2	570	883	1.549	879	1.543	647	1.135	633	1.111	878	1.541
L5-1	700	744	1.062	753	1.075	450	0.643	438	0.626	742	1.060
L5-2	720	757	1.052	767	1.065	455	0.633	443	0.616	756	1.050
L6-1	650	709	1.090	716	1.102	436	0.670	424	0.653	642	0.988
L6-2	570	651	1.142	657	1.152	412	0.723	401	0.704	589	1.033

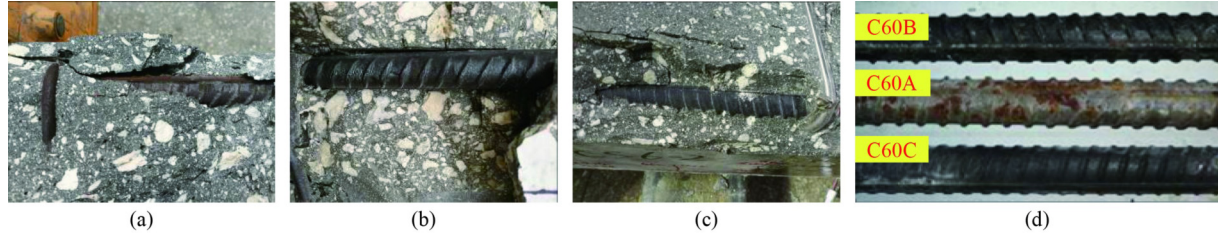


Fig. 11 Steel corrosion status in CAC column: (a) C60A; (b) C60B; (c) C60C; (d) different types of steel.

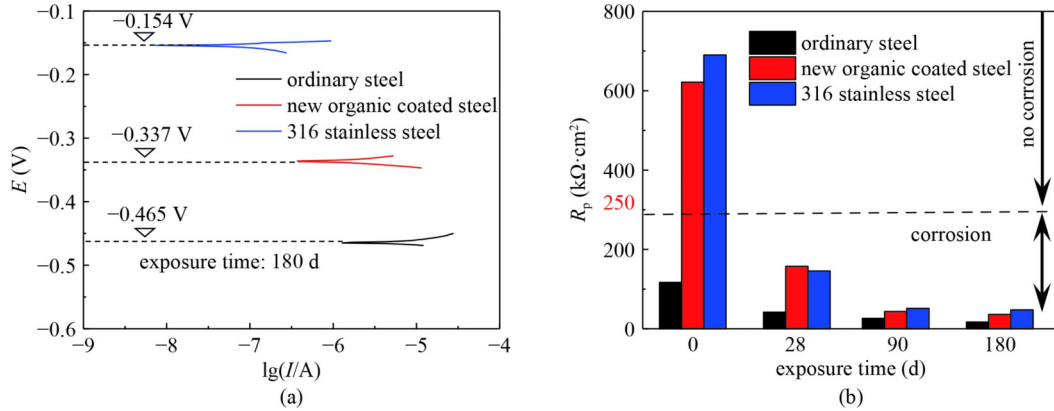


Fig. 12 Electrochemical test result of CAC structural: (a) self-corrosion potential; (b) polarization resistance.

will change the transfer of force in the reinforced concrete structure, keeping the strength of steel bars from playing, and then lead to the bearing capacity of reinforced concrete structure deterioration. In addition, studies have shown that the coated steel surface is covered with a protective layer, and under the load, the steel and concrete in the reinforced concrete column can easily slip [28], thus greatly weakening the mechanical properties of the reinforced concrete column.

In conclusion, considering the effects of steel corrosion and interfacial bond deterioration, the calculation models for the N_u of CAC column is:

1) Axial compression:

$$N_u = k\alpha(\beta_2\beta_3f_cA + f'_yA'_s), \quad (16)$$

where k is steel slip reduction coefficient, coated steel, $k = 0.67$; other steel, $k = 1.0$. See Eqs. (2), (4), and (15) for other parameters.

Using Eq. (16), the N_u of CAC column are shown in Fig. 8 and Table 3. The mean of N_u^c/N_u^t is 1.069, the standard deviation is 0.108, the variation coefficient is 0.101. Compared with the JGJ 12-2006, GB 50010-2010, ACI 318-1999, and EN-1992, the mean more closed to 1, the standard deviations reduced by 77.6%, 80.3%, 52.7%, and 56.7%, the variation coefficient reduced by 70.7%, 73.3%, 47.2%, and 69.7%. Therefore, Eq. (16) is the optimal model.

2) Small eccentric compression:

$$\left\{ \begin{array}{l} N_u \leq k(f_{cm}bx + \alpha(f'_yA'_s - \sigma_sA_s)), \\ N_u e \leq k(f_{cm}bx(h_0 - x/2) + \alpha f'_yA'_s(h_0 - a'_s)), \\ e = \eta e_i + h/2 - a_s, \\ \eta = 1 + \frac{1}{1400(e_0/h_0)} \left(\frac{l_0}{h}\right)^2 \zeta_1 \zeta_2, \\ \zeta_1 = 0.5 f_c A / N, \\ \zeta_2 = 1.3 - 0.015 l_0 / h, \\ e_i = e_0 + e_a, \\ e_a = 0.12(0.3h_0 - e_0), \\ \sigma_s = \frac{x/h_0 - 0.75}{\xi_b - 0.75} f_y, \\ \alpha = \begin{cases} (1 - 1.301\omega)(1 - 1.608\omega), & 0 < \omega \leq 5\%, \\ (1 - 1.301\omega)(0.962 - 0.848\omega), & \omega > 5\%, \end{cases} \end{array} \right. \quad (17)$$

where k is steel slip reduction coefficient, coated steel, $k = 0.78$; other steel, $k = 1.0$; see Eqs. (7) and (16) for other parameters.

Using Eq. (17), the N_u of CAC column are shown in Fig. 9 and Table 4. The mean of N_u^c/N_u^t is 1.028, the standard deviation is 0.038, the variation coefficient is 0.037. Compared with the JGJ 12-2006, GB 50010-2010, ACI 318-1999, and EN-1992, the mean more closed to 1, the standard deviations reduced by 88.2%, 69.4%, 48.3%, and 75.5%, the variation coefficients reduced by 91.1%, 67.3%, 86.4%, and 91.0%. Therefore, Eq. (17) is the optimal model.

3) Large eccentric compression:

$$\left\{ \begin{array}{l} N_u \leq k(\alpha_1 f_c b x + \alpha (f_y' A_s' - f_y A_s)), \\ N_u e \leq k(\alpha_1 f_c b x (h_0 - x/2) + \alpha f_y' A_s' (h_0 - a_s')), \\ e = \eta e_i + h/2 - a_s, \\ \eta = 1 + \frac{1}{1400(e_0/h_0)} \left(\frac{l_0}{h}\right)^2 \zeta_1 \zeta_2, \\ \zeta_1 = 0.5 f_c A/N, \\ \zeta_2 = 1.3 - 0.015 l_0/h, \\ e_i = e_0 + e_a, \\ e_a = 0.12(0.3 h_0 - e_0), \\ \alpha = \begin{cases} (1 - 1.301\omega)(1 - 1.608\omega), & 0 < \omega \leq 5\%, \\ (1 - 1.301\omega)(0.962 - 0.848\omega), & \omega > 5\%, \end{cases} \end{array} \right. \quad (18)$$

where k is steel slip reduction coefficient, coated steel, $k = 0.9$; other steel, $k = 1.0$; see Eqs. (11) and (16) for other parameters.

Using Eq. (18), the N_u of CAC column are shown in Fig. 10 and Table 5. The mean of N_u^c/N_u^i is 1.033, the standard deviation is 0.032, the variation coefficient is 0.031. Compared with the JGJ 12-2006, GB 50010-2010, ACI 318-1999, and EN-1992, the mean more closed to 1, the standard deviations reduced by 20.9%, 18.2%, 21.4%, and 10.0%, and the variation coefficients reduced by 16.8%, 12.9%, 49.2%, and 49.1%. Therefore, Eq. (18) is the optimal model.

4 Conclusions

To study the behavior of coral aggregate concrete (CAC) column under axial and eccentric compression, the compression behavior of CAC column with different types of steel and initial eccentricity (e_i) were tested, and the deformation behavior and ultimate bearing capacity (N_u) were studied. The results were as followed.

1) With the increases of steel strength, the N_u of CAC column increased gradually, indicating that the anti-deformation capacity increased gradually. With the increase of e_i , N_u of CAC column decreased nonlinearly.

2) The steel corrosion in CAC column is severe, which reduces the steel section and steel strength, and decreases the N_u of CAC column. In the loading process, more massive slip takes place between the steel and concrete, the bonding strength decreased, and reduces N_u of the CAC column.

3) The durability of CAC structures can be improved by using new organic coated steel. Considering the influence of steel corrosion and interfacial bond deterioration, the calculation models of N_u under axial and eccentric compression were presented.

Acknowledgements The authors gratefully acknowledge the Project of Young Science and Technology Talents of Jiangsu Province (No. 027), the

Open Funds by State Key Laboratory of Silicate Materials for Architectures (Wuhan University of Technology) (No. SYSJJ2020-19), the Fundamental Research Funds for the Central Universities (No. B210202023), the Water Conservancy Science and Technology Project of Jiangsu Province (No. 2020017), the Open Funds by Key Laboratory of Coastal Disaster and Defense (Hohai University), Ministry of Education (No. 202006), the Systematic Project of Guangxi Key Laboratory of Disaster Prevention and Structural Safety (No. 2019ZDK006), the Postdoctoral Research Funds of Jiangsu Province (No. 2021K133B), the Ningbo Science and Technology Innovation Project (No. 2020Z040).

References

- Da B, Yu H F, Ma H Y, Wu Z Y. Research on compression behavior of coral aggregate reinforced concrete columns under large eccentric compression loading. *Ocean Engineering*, 2018, 155: 251–260
- Wu Z Y, Zhang J H, Yu H F, Ma H Y. 3D mesoscopic investigation of the specimen aspect-ratio on coral aggregate concrete. *Composites Part B: Engineering*, 2020, 198: 108025
- Huang Y J, Li X W, Zhang X C, Ma H. Bond properties of epoxy coated reinforcement to seawater coral concrete. *Journal of Building Materials*, 2020, 23(5): 1086–1092
- Da B, Yu H F, Ma H Y, Tan Y S, Mi R J, Dou X M. Chloride diffusion study of coral concrete in a marine environment. *Construction & Building Materials*, 2016, 123: 47–58
- Wu Z Y, Yu H F, Ma H Y, Zhang J H, Da B, Zhu H W. Rebar corrosion in coral aggregate concrete: Determination of chloride threshold by LPR. *Corrosion Science*, 2020, 163: 108238
- Wattanachai P. A study on chloride ion diffusivity of porous aggregate concretes and improvement method. *Advanced Materials Research*, 2009, 65(1): 30–44
- Zhang W. Experimental study on reinforced coral aggregate concrete component. Thesis for the Master's Degree. Nanjing: Hohai University, 1995 (in Chinese)
- Yu H F, Da B, Ma H Y, Zhu H W, Yu Q, Ye H M, Jing X S. Durability of concrete structures in tropical atoll environment. *Ocean Engineering*, 2017, 135: 1–10
- Da B, Yu H F, Ma H Y, Zhang Y D, Zhu H W, Yu Q, Ye H M, Jing X S. Factors influencing durability of coral concrete structure in South China Sea. *Journal of the Chinese Ceramic Society*, 2016, 44(2): 254–261 (in Chinese)
- Da B, Yu H F, Ma H Y, Wu Z Y. Reinforcement corrosion research based on electrochemical impedance spectroscopy for coral aggregate seawater concrete in a seawater immersion environment. *Journal of Testing and Evaluation*, 2020, 48(2): 1537–1553
- Yang S T, Yang C, Huang M L, Liu Y, Jiang J T, Fan G X. Study on bond performance between FRP bars and seawater coral aggregate concrete. *Construction & Building Materials*, 2018, 173: 272–288
- Ma H Y, Da B, Yu H F, Wu Z Y. Research on flexural behavior of coral aggregate reinforced concrete beams. *China Ocean Engineering*, 2018, 32(5): 593–604
- GB/T 50081-2002. Standard for Test Method of Mechanical

- Properties on Ordinary Concrete. Beijing: Ministry of Construction of the People's Republic of China, 2002
14. JGJ 12-2006. Specification for Design of Lightweight Aggregate Concrete Structures. Beijing: Ministry of Construction of the People's Republic of China, 2006
 15. GB/T 50082-2009. Standard for Test Methods of Long-term Performance and Durability of Ordinary Concrete. Beijing: Ministry of Housing and Urban-Rural Development of the People's Republic of China, 2009
 16. GB/T 50152-2012. Standard for Test Method of Concrete Structures. Beijing: Ministry of Housing and Urban-Rural Development of the People's Republic of China, 2012
 17. Yuan Y S, Jia F P, Cai Y. The structural behavior deterioration model for corroded reinforced concrete beams. *China Civil Engineering Journal*, 2001, 34(3), 47–52 (in Chinese)
 18. Pujol S, Hanai N, Ichinose T, Sozen M A. Using Mohr–Coulomb criterion to estimate shear strength of reinforced concrete columns. *ACI Structural Journal*, 2016, 113(3): 459–468
 19. ACI 318-1999. Building Code Requirements for Structural Concrete. Farmington Hills: American Concrete Institute, 1999
 20. JGJ 12-2006. Technical Specification for Lightweight Aggregate Concrete Structures. Beijing: Ministry of Construction of the People's Republic of China, 2006
 21. GB 50010-2010. Code for Design of Concrete Structures. Beijing: Ministry of Housing and Urban-Rural Development of the People's Republic of China, 2010
 22. EN-1992. Code for Design of Concrete Structures. Brussels: European Committee for Standardization, 1992
 23. Da B, Yu H F, Ma H Y, Tan Y S, Mi R J, Dou X M. Experimental investigation of whole stress–strain curves of coral concrete. *Construction & Building Materials*, 2016, 122: 81–89
 24. Da B, Yu H F, Ma H Y, Zhang Y D, Yuan Y F, Yu Q, Tan Y S, Mi R J. Experimental research on whole stress–strain curves of coral aggregate seawater concrete under uniaxial compression. *Journal of Building Structures*, 2017, 38(1): 144–151 (in Chinese)
 25. Zhang W P, Zhou B B, Gu X L, Dai H C. Probability distribution model for cross-sectional area of corroded reinforcing steel bars. *Journal of Materials in Civil Engineering*, 2014, 26(5): 822–832
 26. Wang X H, Zhong T Y. Relation between the loss coefficient of the corroded rebar's cross-section in concrete and that of its weight. *Research and Application of Building Materials*, 2005, 1(4): 4–6 (in Chinese)
 27. Zhao Y X, Lin H W, Wu K, Jin W L. Bond behaviour of normal/recycled concrete and corroded steel bars. *Construction & Building Materials*, 2013, 48: 348–359
 28. Kivell A, Palermo A, Scott A. Complete model of corrosion-degraded cyclic bond performance in reinforced concrete. *Journal of Structural Engineering*, 2015, 141(9): 04014222